J Ther Eng, Vol. 11, No. 5, pp. 1585−1599, September, 2025

Journal of Thermal Engineering
Web page info: https://jten.yildiz.edu.tr
DOI: 10.14744/thermal.0000994

Review Article

Factors affecting and methods of reducing thermal stratification in cryogenic storage tanks of launch vehicles: review article

Krish V. RAIBOLE[1], Puskaraj D SONAWWANAY[1,*]

[1]*Department of Mechanical Engineering, Dr. Vishwanath Karad MIT World Peace University, 411038 Pune, India*

ARTICLE INFO

Article history
Received: 22 June 2024
Revised: 23 October 2024
Accepted: 27 October 2024

Keywords:
Cryogenic Propellants; Launch Vehicles; Liquid Rocket Engines; Thermal Insulation; Thermal Stratification

ABSTRACT

Contemporary launch vehicles of the past few decades primarily implement liquid rocket engines, which in turn employ cryogenic propellants stored in sub-zero conditions in highly sophisticated cryogenic storage tanks. These tanks are usually deprived of any thermal insulation in order to prioritize the payload capacity, and thus they are prone to a substantial amount of heat in-flux that leads to a rise in the temperature of the cryogenic liquid, leading to thermal stratification. This paper presents a comprehensive review of the various factors affecting the rate of thermal stratification in cryogenic propellant storage tanks, along with numerous experimental and numerical techniques developed for controlling or mitigating this stratification through geometrical modifications, varying surface properties, and bubbling of gases through the bulk liquid. Out of the techniques reviewed, simple geometrical modifications showed substantial results, with ribs reducing stratification by up to 30%. On the other hand, complex techniques like bubbling of gases destratified the bulk liquid within 25 to 35 s. A special focus has also been placed on reviewing the numerical modelling and simulations of this phenomenon, particularly those developed in recent years.

Cite this article as: Raibole Krish V, Sonawwanay Puskaraj D. Factors affecting and methods of reducing thermal stratification in cryogenic storage tanks of launch vehicles: review article. J Ther Eng 2025;11(5):1585−1599.

INTRODUCTION

Nearly every sophisticated launch vehicle of the 20th century employs cryogenic propulsion systems [1]. Therefore, understanding the complications involved in such systems is of utmost importance. One such difficulty arises in the storage of such low temperature liquids. Storage and transportation of such low temperature cryogenic liquids has always been one of the primary challenges in its application [2,3]. Cryogenic liquids, with temperatures in the range of -187 °C to -210 °C, are primarily stored inside cylindrical tanks that receive heat from the surroundings, causing a subsequent change in density and temperature variance between the bulk and liquid adjacent to the walls [4–6]. This leads to the formation of convective currents, wherein warm layers, comparatively less dense, rise up and accumulate near the liquid vapour boundary, resulting in the formation of a temperature rise along the height of the tank as illustrated in Fig. 1 [7,8]. The accumulated liquid near the interface is called 'thermal

*Corresponding author.
*E-mail address: puskaraj.sonawwanay@mitwpu.edu.in

This paper was recommended for publication in revised form by Editor-in-Chief Ahmet Selim Dalkılıç

stratified liquid', and this phenomenon is called 'thermal stratification'. Apart from thermal stratification occurring due to convection currents developed in the bulk liquid, heat flux from the hotter ullage can also augment thermal stratification. This phenomenon has also been reported to persist in launch vehicles in both, sea-level and micro-gravity levels [9–11]. Furthermore, the pressure of the vapor phase, known as the ullage (Refer Fig. 1), also dictates the degree of stratification [12,13]. Fig. 1 depicts the phenomenon of thermal stratification in a cryogenic storage tank, wherein, under the action of buoyancy force, natural upward convection currents are developed, which result in the formation of boundary layers along the tank walls [14,15]. T_S, T_B & T_U stand for the temperature of the stratified layer, bulk liquid and ullage, respectively, and their typical ranges in a cryogenic storage tank are shown in Fig.1.

Thermal stratification of the fuel, typically LH_2, is a highly unfavourable phenomenon that affects the functioning of the cryogenic engine, even if the temperature difference is only of a few degrees [16–18]. Any degree of stratification, if present, affects the system negatively [19]. It results in an increase in the pressure of the vessel, conforming to the temperature of the warmer upper layers of the fuel (LH_2). To maintain the required tank pressure, the vapor formed due to stratification has to be vented out. In the case of LH_2 as the fuel, its stratification would lead to diminished lock-up times, implying that the time required for the vaporized LH_2 gas pressure to reach the tank's pressure limit would be reduced; and the warmer stratified column of LH_2 would source cavitation inside the LH_2 pumps [20,21]. Subsequently, a plethora of techniques have been implemented in the past to counter stratification, such as: baffles, fins, and ribs on the tank's inner wall [22–24], mixers [25–27], bubbling of gases [28], etc. These techniques have been discussed in detail in further sections.

Owing to the importance of comprehending thermal stratification and a lack of detailed review articles on the same, the present study provides a comprehensive review of research spanning over 60 years involving a wide array of techniques employed to mitigate thermal stratification in cryogenic liquids. The present study explores numerous destratification techniques employed which have not been comprehensively reviewed before. The scope of this study involves delineating various factors that influence thermal stratification in cryogenic liquids, followed by the different numerical and experimental approaches adopted by researchers in the past half-century. The scope of this study is not only limited to the stratification dynamics involved in the storage tanks of launch vehicles, but is also applicable to the transportation and storage of cryogenic liquids in the thermal, power and energy sector. Furthermore, experimental techniques employed to mitigate stratification have also been extensively reviewed. Special care has also been taken to include recent trends observed in studies involving thermal stratification. The present study, will not only help researchers and readers to get an in-depth picture of the works conducted on the thermal stratification in the last half a century, but also aid in highlighting research efforts necessary to be taken in the future.

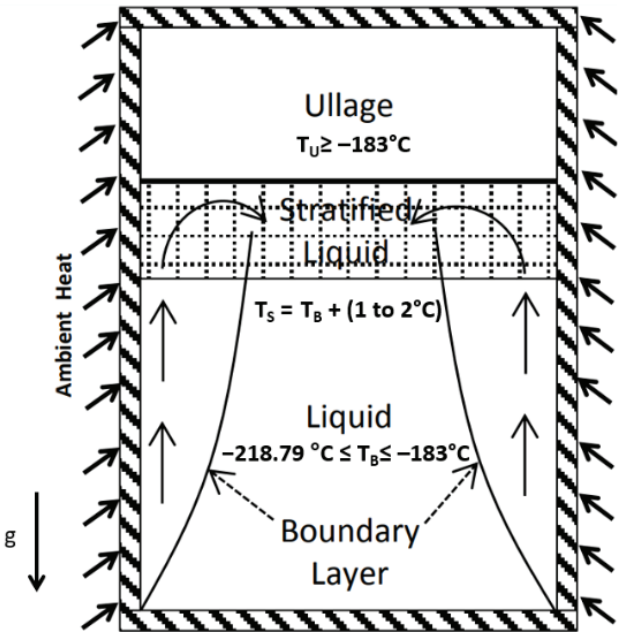

Figure 1. Representation of liquid stratification phenomenon inside a cryogenic tank [From Agarwal et al. [14], with permission from IOPscience.]

FACTORS AFFECTING THERMAL STRATIFICATION

The following section enumerates various real-world parameters that significantly affect the degree of stratification in storage tanks of LVs. Owing to their importance, only the parameters which are experienced by a LV during its mission, have been explained in detail below.

Effect of Rotation of Launching Vehicle

After lift-off, just after the LV clears the launch tower, a rolling motion of the LV about its vertical axis is initiated through thrust vectoring or, in the case of sounding rockets, by the use of canted fins, which produce aerodynamic forces. These forces are applied at the centre of pressure of the rocket, which is at some distance from the rocket's centre of gravity, resulting in a torque (or moment) about the major axes, as seen in Fig. 2. This torque causes the rocket to rotate about the axis, initiating a roll manoeuvre [29,30].

The rotation, in turn, has an effect on the motion of the fluid inside the tanks. It is assumed that the liquid has a solid body rotation and takes a paraboloid shape, resulting in an increased contact surface area between the liquid and the tank walls, as seen in Fig. 3 [31–33]. Fig. 3 represents a similar case wherein the gravitational force is perfectly aligned with the rocket, acting vertically downward. It is

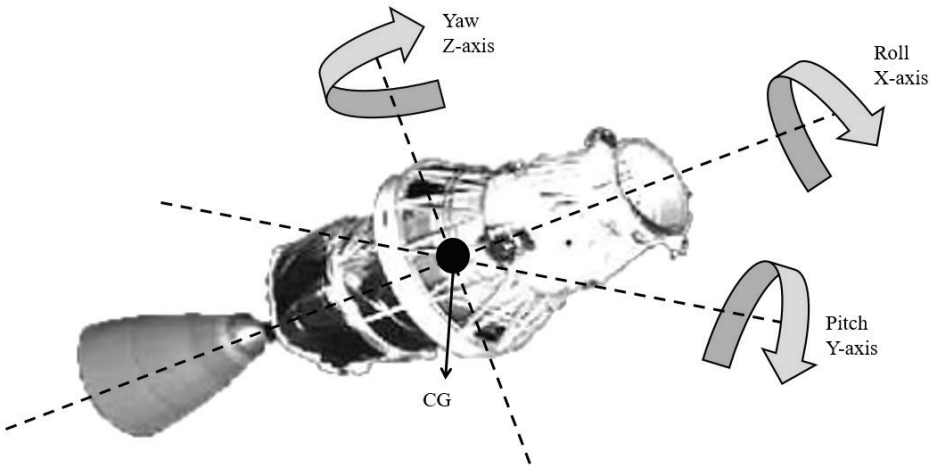

Figure 2. Principal axis of rotation of the LV [From Oliveira et al. [29], with permission from NASA NTRS]

evident from Fig. 3 that the liquid at the center of rotation dips down by a height equal to the height of the liquid that rises at the rim, given by (h/2), where h represents the distance between the lowest and highest points of liquid at the surface. The liquid within the tank is observed to have a similar significant dishing effect [14]. Fig. 4 depicts a combined model of rotation and stratification, illustrating the effect of different gravity levels on the shape attained by the liquid fuel (LH_2) surface. This displays how a parabolic surface of the liquid results in the liquid gaining height along the tank wall, resulting in a higher net heat transfer from the wall to the liquid as illustrated in Fig. 3 & 4. At a spin rate of Ꞷ= 1 °/sec and at reduced gravity levels of up to $g/g_0 = 10^{-5}$ the liquid is observed to be parabolic in shape, as seen in Fig. 4 [34]. The resultant tank temperature always tends to be higher because of the larger ΔT**,** with increasing rotation. Rotation has a large impact on stratification as it is observed to reduce the time required for stratification of

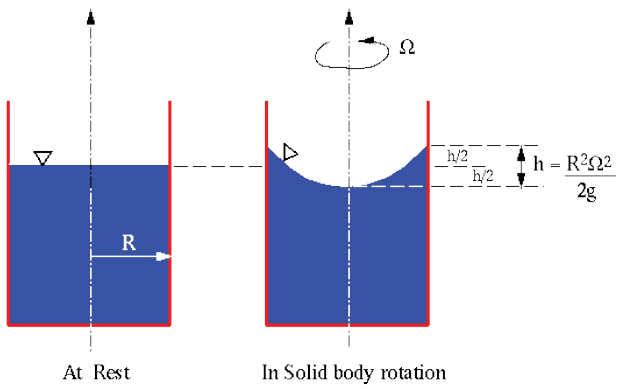

Figure 3. Paraboloid of revolution liquid free surface [From Cimbala et al. [83], with permission Penn State University.]

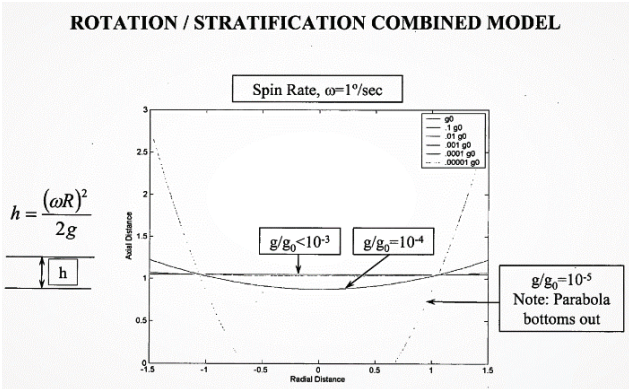

Figure 4. Rotation/Stratification combined model [From Oliveira et al. [29], with permission from NASA NTRS.].

LH_2 stored in a square tank of 3 m in diameter at 20% fill level at 16 K and 206843 Pa with a heat flux of 10 W/m² by 30 to 60 minutes during the 4 hr coast phase of the LV, which is rotating at Ꞷ= 1 °/sec in $g/g_0 = 10^{-4}$. Overall, the effect of rotation on stratification for the boundary conditions mentioned above is observed as follows:

- Rotation reduces period to stratification by 15%.
- Rotation intensifies stratification temperature by 1.0 K [29,30,32,33].

Effect of Insulation Thickness

The insulation thickness of a cryogenic tank wall is a critical specification that influences the entire mission of the LV [35]. Excess insulation thickness results in extra weight added to the LV, hindering its efficiency. On the other hand, insulation thickness that is lower than what is required, results in excess heat flux into the liquid from outside the tank [36,37]. This, in turn, increases the stratification rate

of the fluid as seen in Fig.5 [38]. The optimum insulation thicknesses of several types of materials, like Extruded polystyrene (EXS), Expanded polystyrene (EPS), and rock wool, have been determined in the past and show promising results in limiting the heat in-flux from the side walls of cylindrical tanks [39,40].

Thermal stratification in the liquid and stratified mass growth inside a LH_2 storage tank in ambient conditions, which is of diameter 4 m, 7 m in length, and a wall thickness of 4 mm, for varied thickness of insulation, can be observed in Fig. 5, wherein the temperature of the pressurant gas used was 50 K. The thickness of the foam-based insulation varies from 10 mm to 40 mm, as 10 mm, 20 mm, 30 mm and 40 mm whereas the liquid fill level was kept constant at 87% of the total tank height [38]. The heat in-leak for tanks of different insulation thicknesses is observed in Fig.6. Heat in-leak is plotted for two different times, t = 300 s, which covers the time taken for pressurisation, and t = 600 s, which covers an extended time of 300 s after pressurisation is completed.

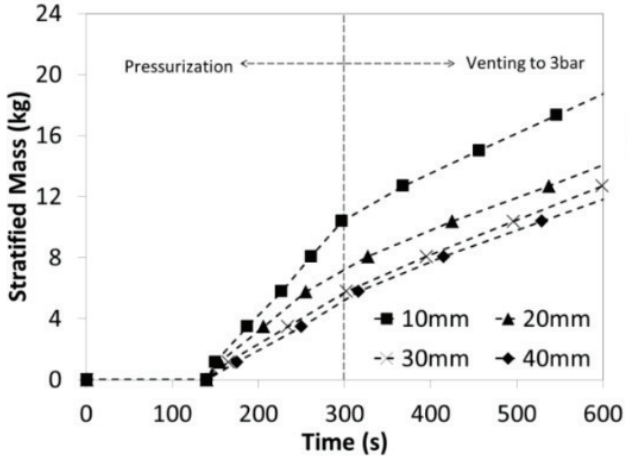

Figure 5. Stratified mass (kg) Vs. Time (s) [From Joseph et al. [38], with permission from Elsevier.].

It is evident from Fig. 6 that the tank with the highest insulation thickness of 40 mm records a heat in-leak of only 10.7 W/m^2. Ullage temperature, as reported for all cases of insulation thickness, was in the range of 21 to 45 K before pressurisation. Thus, the warm pressurant gas entering the tank at 50 K leads to an increase in the ullage gas temperature. This results in the ullage gas temperature being higher than the wall temperature, culminating in a net heat loss to the tank wall. This is exhibited in Fig. 6, wherein the heat in-leak for t= 300 s is negative [38]. Lesser thickness of tank insulation leads to higher stratified mass due to higher liquid heat in-leak from the surroundings, triggering a payload penalty in propellant tanks used in launch vehicles as observed for a thickness of 10 mm, which resulted in a heat in-leak of 64.3 W/m^2, as shown in Fig. 6 [38,41].

Effect of Pressurization

Pressurization occurs in two stages, the first being wherein the tank is pressurised to reach the required tank pressure. While the second stage involves maintaining the required tank pressure with the use of pressurant gas. Similarly, it is observed that throughout pressurization the stratified mass increases at a quicker rate compared to that during the fixed pressure scenario post pressurization (Fig. 5) [42].

This is due to the fact that during the pressurization phase, there is a continuous increase in the liquid-vapor interface temperature corresponding to the saturation temperature at that pressure, which is a result of the ullage temperature being higher during pressurisation [43]. During this phase, the stirring effect produced by the pressurant gas results in an enhanced forced convective heat transfer

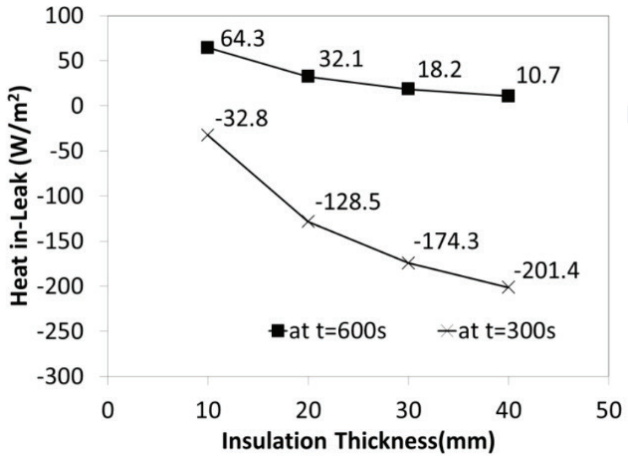

Figure 6. Heat in-leak (W/m^2) Vs. Insulation Thickness (mm) [From Joseph et al. [38], with permission from Elsevier.].

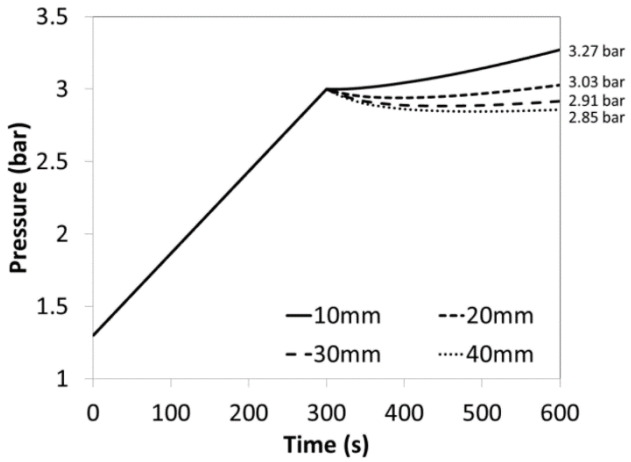

Figure 7. Pressure rise for different insulation thicknesses during and post pressurisation [From Joseph et al. [38], with permission from Elsevier.]

coefficient between the ullage and the liquid-vapor interface. Due to this, there is an increment in the conductive heat flux from the liquid-vapor interface to the bulk liquid inside the tank, as illustrated in Fig. 7. Apart from this, there is an additional temperature rise due to the ambient heat in-leak into the tank in spite of the insulation layer [44–51].

Fig. 7 depicts how the ullage pressure rises during pressurisation (t = 300 s) and after pressurisation is completed (t = 600 s). The cooling of ullage gas after pressurisation accounts for the pressure drop after t = 300 s, as seen in Fig.7. A subsequent rise in pressure is observed due to heat in flux from the tank wall to the ullage, which dominates its cooling rate [38]. Hence, for lower insulation thicknesses, there is a greater heat in flux, leading to a higher pressure rise than thicker insulations as illustrated in Fig. 7. Hence, it is detected that tank pressure has a noteworthy role in the rate of thermal stratification or stratified mass evolution. Higher tank pressure causes more mass of the liquid to be stratified, and vice versa.

Similarly, in 2019, Vishnu et al. [52] evaluated the development of thermal stratification, experimentally and numerically, and its effects on tank self-pressurization, in a 10 L stainless steel tank of 1400 mm height and 108 mm in diameter, filled with liquid Nitrogen up to a height of 660 mm. The tank wall consisted of a total of 30 layers of fiberglass paper and foils of aluminium placed alternatively. An outer vessel of 400 mm in diameter served as a vacuum heat shield to minimize the heat in-leak. Stratification was measured using PT100 temperature sensors, which were placed along the height of the tank. The experimentation was carried out under two tank conditions, namely venting and non-venting. Venting implied that the vent valve was kept open all throughout the experiment, whereas in the non-venting case, the valve remains shut, leading to the tank's self-pressurization. For the venting case, negligible thermal stratification was observed even after a time of 2000 seconds, with a maximum temperature difference of 1.03 K between the uppermost and the bottommost layer of the liquid. On the other hand, the non-venting case showed a temperature difference equivalent to 6 K, which can be attributed to the rise in pressure of the ullage. It was also reported that the rate of thermal stratification at the gas-liquid interface was greater than the stratification rate of the bottommost layer. This is the result of an ascending convection current formed within the bulk liquid due to the effect of buoyancy.

For the non-venting case, as the tank pressure was increased from 1 to 4 bar, stratification was observed to increase throughout the liquid as evident from Fig. 8. The interface temperatures for the pressures of 1,2,3 and 4 bar, were reported to be 79.8 K, 81.3 K, 83.3 K and 87.4 K, respectively, as seen in Fig. 8 [52]. A stratification parameter (λ) was established in an attempt to quantify the degree of stratification. λ is given by Eq. (1):

$$\lambda = \frac{T_8 - T_1}{T_0} \quad (1)$$

Wherein, T_8 and T_1 stand for the temperature readings recorded by the eighth sensor and first sensor from the tank's bottom, respectively [52]. In total, 16 sensors are placed along the height, with eight lying at the liquid-gas interface. For the venting case, this parameter stayed near constant and averaged at a value of 0.015 after a duration of 25 min. Whereas, in the case of the non-venting condition, λ increased from 0.0275 at t=0 min and reached a value of 0.045 after 25 min. Furthermore, Vishnu et al. [52] also developed a numerical model to further understand the complexities of the thermodynamics involved.

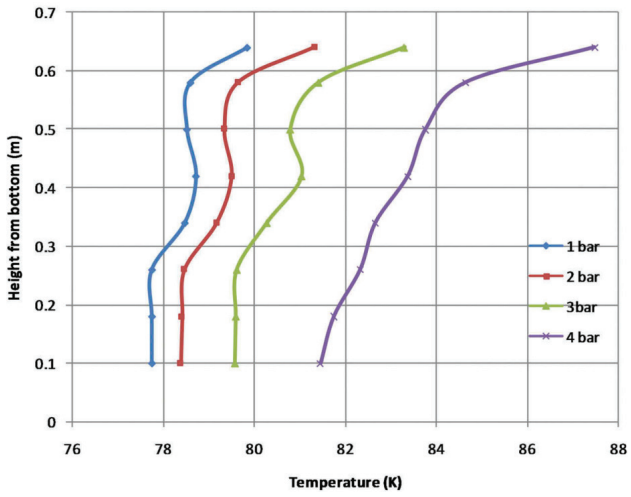

Figure 8. Development of stratification by varying tank pressure from 1 to 4 bar [From Vishnu et al. [52], with permission from Taylor & Francis.]

NUMERICAL MODELLING

As the numerical modelling schemes and techniques improve over time, research in the domain of aerospace and thermodynamics has gradually inclined more and more towards incorporating these numerical simulations in order to better understand the underlying complexities involved. A similar trend has been observed in evaluating the thermal stratification occurring in cryogenic tanks [53].

Various mixing techniques, such as sprinklers [54], rotating tank lids [55], porous structures [56–58] and nozzle jets [59], have been experimentally and numerically investigated in the past and have exhibited encouraging results in disrupting the natural convective flows in the bulk liquid. Similarly, in 2024, Brodnick et al. [60] numerically modelled and validated an axial jet mixer in order to attain a homogeneous temperature across the cryogenic propellant. The aim of using a jet mixer within the propellant tank is to induce a swirling current within the bulk fluid, which results in enhanced forced convection leading to a more homogenous temperature of the propellant along with a

reduced ullage pressure. Fig.9 (a) shows the tank design, and Fig.9 (b) illustrates the computational domain (1.2 major-to-minor axis ratio with a major diameter of 2.2 m) incorporating the axial jet mixer. The jet mixer was modelled such that its tip had a rounded lip design as illustrated in Fig.9 (a). A fill level of 86% of the tank's total volume was used in this study [60].

Loci/STREAM was the CFD code employed by Brodnick et al. [60] and served as a pressure-based solver for the simulations. Instead of applying the VoF (Volume of Fluid) method, an interface model known as the sharp interface model, specially designed for the Loci/STREAM solver was implemented. A total of 119,700 cells were used to discretize the domain while solving equations with 1st and 2nd order accuracy in time and space, respectively, with a time step size equal to 0.1 s. Buoyancy within the liquid phase was modelled by employing the Boussinesq approximation. For modelling the turbulence, the 2 equation $k-\omega$ SST model was chosen. A heat flux of 4.2 W/m^2 was provided to the tank walls as an initial boundary condition. The effect of jet flow rate was studied by varying the flow rate from 1.82 m^3/hr to 3.47 m^3/hr [60].

Fig. 10 demonstrates the destratification results obtained for the jet mass flow rate of 3.47 m^3/hr. From Fig.10 it can be clearly observed that, after a time of 8 min has passed, due to the mixing induced by the jet, thermal stratification within the liquid is virtually nullified. As anticipated, the case with the higher jet flow rate provided better and more promising results than the low flow rate case. From the initial ullage pressure of 186.1 kPa, the higher jet mass flow rate took nearly 8.3 min to drop the ullage pressure to a pressure of 128.4 kPa as represented in Fig. 10. Whereas, the lower jet mass flow rate took more than 20 min to accomplish the same pressure drop [60].

Similarly, in 2024, Raj et al. [61] numerically analyzed the rate of thermal destratification by bubbling of gases in liquid storage tanks with the help of a newly developed OpenFOAM solver, interThermalDestratificationFoam, that was specially designed to solve thermal stratification

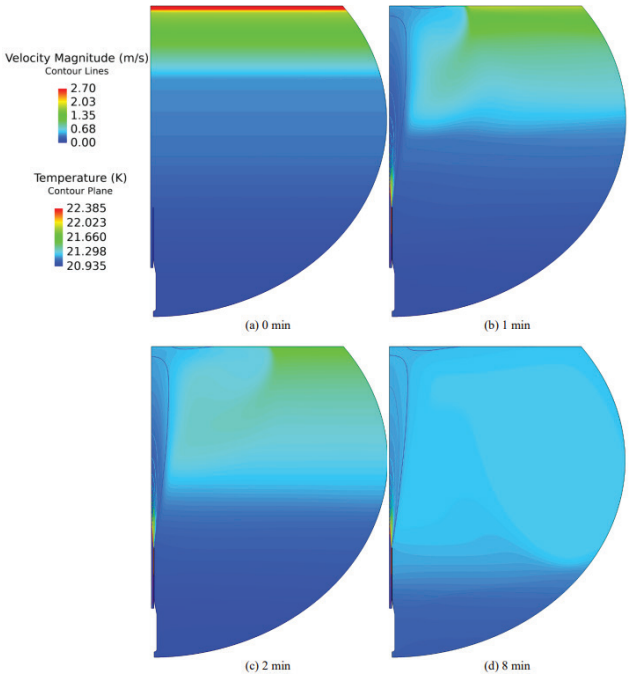

Figure 10. Temperature contour of the propellant fill level at a jet mass flow rate of 3.47 m^3/hr [From Brodnick et al. [60], with permission from NASA NTRS.]

problems. In this study, primarily two cases were compared, both in 2D and 3D: a tank with one orifice and a tank with two orifices. To obtain a comprehensive understanding of the decay in stratification and its effect on gas bubble dynamics, fluid properties such as interfacial tension force, liquid viscosity and density were varied as shown in Table 1.

Fig. 11 shows the 2D computational domain with a singular orifice used by Raj et al. [61]. The rectangular tank measured 100 mm by 50 mm with a fill level up to a height of 85 mm. The orifice had a diameter of 0.3 mm and in the case of 2 orifices, they were placed 12.5 mm apart from each other. In order to satisfy the CFL (Courant Frederick-Levy) criteria,

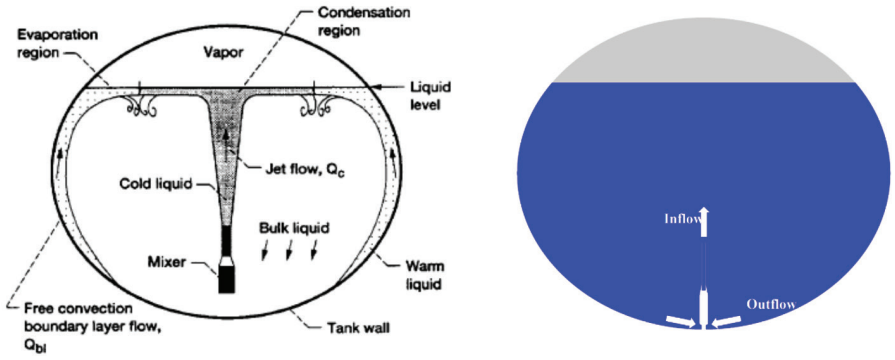

Figure 9. Cryogenic tank design with the axial jet mixer [From Brodnick et al. [60], with permission from NASA NTRS.]

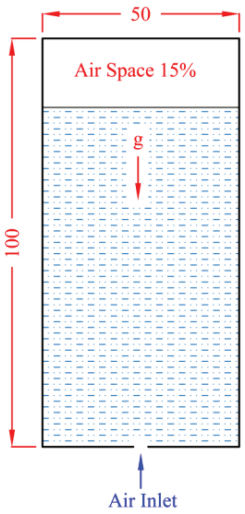

Figure 11. 2D Computational domain [From Raj et al. [61], with permission from Elsevier.]

the time step for the simulations was adjusted and reduced to 0.15 ms for the 2D simulations, whereas for the 3D simulations, a time step of 0.1 ms was implemented. When one parameter was changed, the other parameters were kept constant for simplicity purposes as tabulated in Table 1.

For the 3D domain, a cylindrical tank (diameter = 50 mm) of 162 mm height, with liquid filled up to a height of 152 mm was modelled with an orifice diameter of 2 mm. Results for the 2D case, indicated an increase in the bubble diameter and the bubble's detachment time with respect to reducing surface tension values. After a time of t = 0.44 s, σ = 0.0728 N/m showed 5 distinct detached bubbles, whereas for the case of σ = 0.0482 N/m, 6 bubbles were reported. A similar result was observed for dynamic viscosity, wherein bubble diameter and detachment time increased with an increase in the liquid's viscosity. With increasing liquid density, the rate of bubble detachment was also reported to rise [61,62].

To quantify thermal destratification efficiency in the 3D case, a thermal stratification decay coefficient (T_{sd}) is defined. T_{sd} is given by Eq. (2):

$$T_{sd} = \frac{|T_{fin} - T_{ini}|}{t_{ho}} \quad (2)$$

T_{fin} represents the resulting temperatures of the liquid layers post bubbling of gases, whereas T_{ini} represents the initial temperature of the liquid layers and t_{ho} is the time required in seconds to achieve a homogeneous temperature within the liquid. Consequently, as anticipated, the value of T_{sd} and T_{sdavg} for the inlet gas velocity of 0.8 m/s was the highest, and the time required to achieve a uniform temperature distribution in the liquid was 24.95 s. This is illustrated in Fig. 12 below. T_{sdavg} is defined as the spatially averaged value of T_{sd} at every instant for every case [61].

Similarly, Fig.13 depicts the gradual development of destratification within the bulk liquid with progressing time for the single inlet case and an inlet gas velocity of 0.6 m/s. A time of 27.73 s is required to attain a uniform temperature distribution in the liquid when an inlet gas velocity of 0.6 m/s is provided [61].

This investigation conducted by Raj et al. [61] on the effects of various parameters on the rate of thermal

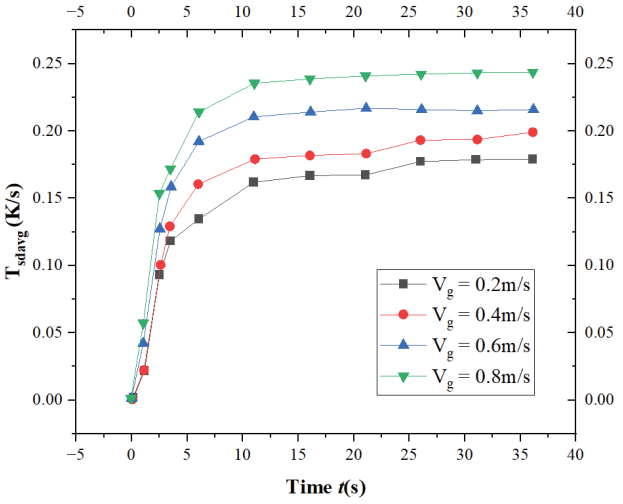

Figure 12. Variation of T_{sdavg} with time for different gas inlet velocities [From Raj et al. [61], with permission from Elsevier.].

Table 1. Variation of parameters for the 2D and 3D case [From Raj et al. [61], with permission from Elsevier.]

Parameter	Value 1	Value 2	Value 3	Value 4
2-Dimensional case				
Surface tension (N/m)	0.0728	0.0693	0.0538	0.0482
Bulk liquid density (kg/m^3)	998.2	1500	2000	2500
Viscosity (Pa-s)	3.494×10^{-06}	7.203×10^{-06}	1.1698×10^{-05}	1.501×10^{-05}
3-Dimensional case				
Inlet gas velocity V_g (m/s)	0.2	0.4	0.6	0.8

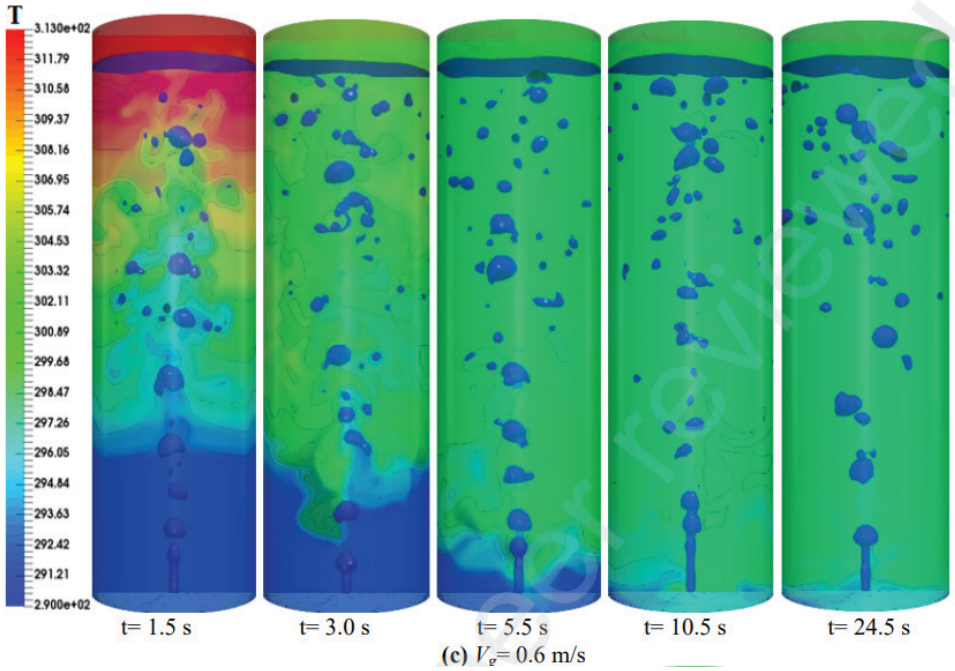

Figure 13. Thermal destratification as a result of gas bubbling for v=0.6m/s [From Raj et al. [61], with permission from Elsevier.].

destratification serves as an intermediate step in designing an efficient cryogenic tank with minimum stratification.

EXPERIMENTAL STUDIES

Methods of Reducing Thermal Stratification

A number of techniques effective in mitigating stratification have been discussed in detail in the following sections. These techniques either involve modifying the tank's geometry or introducing external elements, such as a mixer or bubbling inert gasses through the bulk liquid. The scope of the following sections, involves delving into promising experimental techniques that have been employed in the recent past to deter stratification. The methods have been explained in detail below, as follows:

Surface Roughness Elements

Surface roughness of the tank's inner walls is a key element in determining the amount of stratification that might occur within the liquid. Micro-surface irregularities have little to no effect on the rate of stratification, although more prominent features like ribs and isogrid walls have a significant effect on stratification. Ribs on the inner walls of the tank are an effective way of reducing stratification, as it enhances the mixing of the fluid layers within the tank.

Fig. 14 shows a cross section of a cylindrical tank of height 'H' and diameter 'D'. Roughness elements are introduced on the cylindrical wall of the tank in the shape of ribs having rectangular cross-section of height 'h' and spaced apart by distance 'p' [20]. Stratification mainly occurs in three stages, which are as follows; Stage 1: Formation of a boundary layer along the wall, leading to lateral intervention of the warmer liquid adjacent to the upper region. Stage 2: Series of intricate interactions occur amid the thermal boundary layer and the bulk. Stage 3: Final stage comprises the development of a stratified column of the liquid

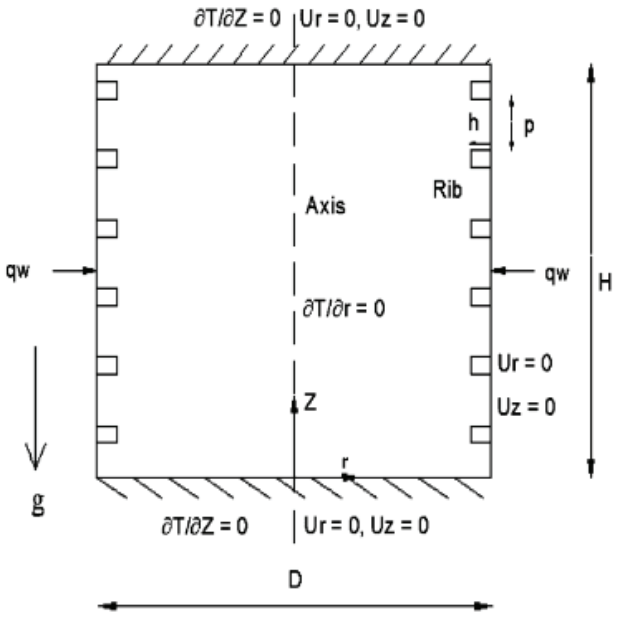

Figure 14. Physical illustration of a ribbed cylinder-shaped tank [From Khurana et al. [20], with permission from Elsevier.]

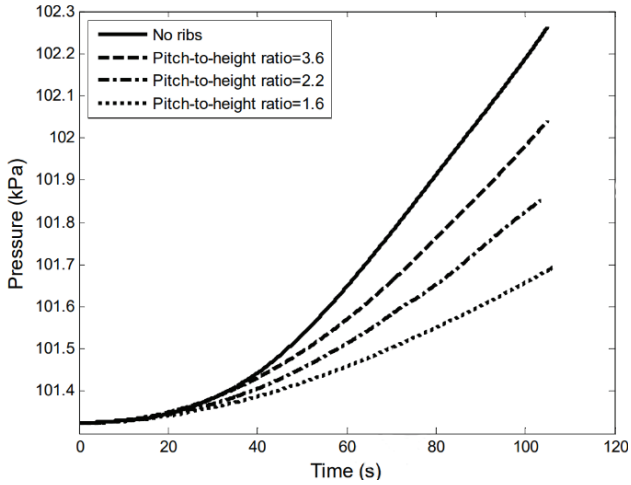

Figure 15. A comparison of pressure rise with time for tank with different rib configurations [From Fu et al. [63], with permission from Elsevier.]

inside the tank, resulting in a temperature gradient along the height of the tank. It is observed that for tanks having ribbed surfaces as shown in Fig. 14, the time essential for the formation of the thermal boundary layer [Stage 1] is higher as compared to tanks with smooth walls. The time required further increases with increase in the ratio of the height of the rib to the spacing amongst two ribs (h/p) as shown in Fig. 15. Although it does not have a major effect on the degree of stratification [20].

Fig.15 above shows the evolution of pressure with time for a tank with ribs with 3 different pitch-to-height ratios of 3.6, 2.2 & 1.6, compared to a tank with a smooth inner wall [63]. It is evident that the rate of pressure increase is minimum for a pitch-to-height ratio of 1.6, while it is the highest for a tank with no ribs. Hence, as discussed in the previous section (Section 2.3), a lower rate of pressure rise is preferred for lesser stratification. Fig.16 below shows the nomenclature used to define different surfaces of the ribs along with their respective wall heat transfer coefficients.

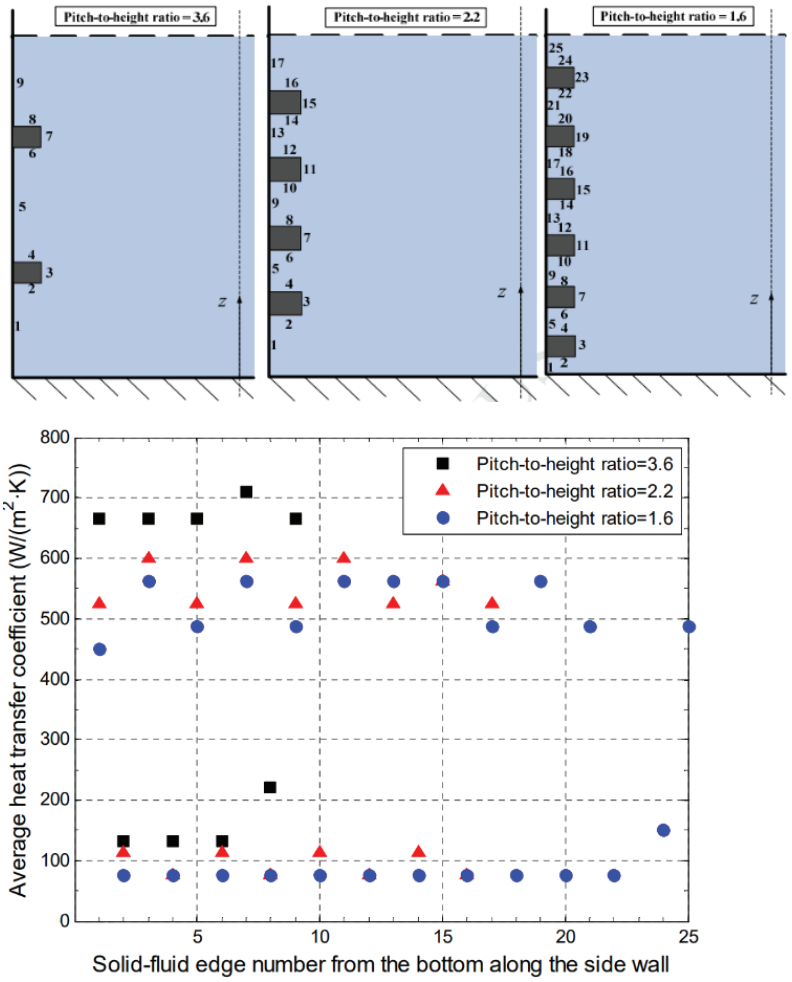

Figure 16. A comparison of the heat transfer co-efficients of different surfaces of the rib and tank wall [From Fu et al. [63], with permission from Elsevier.]

As the number of ribs are increased, so does the number of solid-liquid interfaces within the tank. For pitch-to-height ratios of 1.6, 2.2 and 3.6 there are 25, 17 and 9 surfaces, respectively, as shown in Fig. 16. It is evident that the upper and lower surfaces of each rib have a lower heat transfer coefficient, typically observed to be in the range of 50 to 160 W/m^2K as shown in Fig. 16. This is due to the fact that the ribs serve as an obstruction to flow velocity, leading to the thickening of the boundary layer around its surfaces [63].

Overall, the presence of ribs on the internal wall drastically reduces the degree of stratification by almost as much as 30%. Such ribs essentially slow down the convection currents formed within the liquid and act as dampers for all stages of stratification [20,63,64]. Consequently, very recently, ribs of different configurations like V-shaped ribs [65,66], micro-ribs [67,68] and cylindrical ribs [69–72] have also been extensively studied, owing to their enhanced heat transfer qualities.

Modifying Geometry of The Tank

The introduction of a circular or parabolical bulkhead above the total height of the cryogenic tank helps disrupt the natural convection flow of the liquid along the periphery of the tank. Although this method is successful in reducing the stratification rate significantly, it is not preferred due to the complexities involved in the design phase. Another promising method involves the introduction of baffles on the inner walls of the tank [57,58,72–79]. Fig.17 illustrates the use of such baffles along the tank walls.

The tank in Fig.17 is cylindrical in shape, with a diameter of 201 mm and a height of 213 mm respectively. It has two annular plane baffles fitted along its internal wall. The effect of such baffles was studied through a two-dimensional Volume of Fluid (VOF) simulation conducted in reduced gravity environments of $10^{-5}g_0$, $10^{-3}g_0$, $10^{-1}g_0$, respectively. 'd' is defined as the linear distance amid two neighboring baffles, which was varied from 0 to 60 mm, wherein 0 mm signified a single baffle. The two baffles are positioned symmetrically along the center of the tank. Symbols θ and δ are defined as the angles amongst the baffle and the tank wall, as shown in Fig. 17, which were θ_1=105° and θ_2= 75° for one case and vice versa for the other; and the gap between the baffle and the wall, varied as 5 mm and 10 mm; respectively. d, θ and δ were varied in order to optimise the effect of baffles on suppressing flow velocity and pressure. The effects of different fill levels (30% to 70%) were also investigated and it was reported that for fill levels between 40% and 60% wherein the baffles are fully immersed in the liquid phase, the pressure rising rate in the simulated tank is considerably lower, than in a tank without baffles [44].

As gravity reduces from $10^{-1}g_0$ to $10^{-5}g_0$, the convection current below the baffles is augmented. A very similar phenomenon was observed in the vapor phase of the ullage. Subsequently, the temperature stratification in the fluid deteriorates. This can be attributed to the suppression of hot-spots which cause the local superheating of the liquid with a reduction in gravity [44].

It was observed that to improve the suppression of sloshing and pressurization within the tank, a large distance of 60 mm between the baffles was preferred over 40 mm. Fig.18 illustrates the variation in the pressure rise for baffles with varying distance between adjoining baffles. 60 mm baffle distance showed a 47% lower pressure rise than for the case of 40 mm as shown in Fig.18 above. Installation of such baffles also leads to disruption of the natural convection flow in the tank [44,71,74].

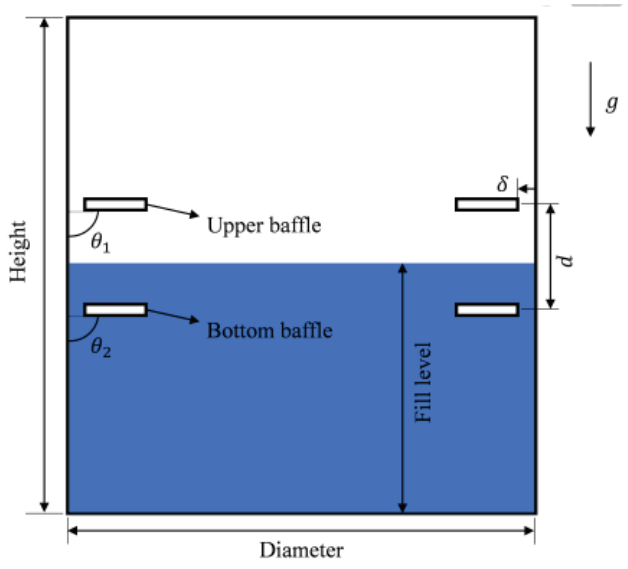

Figure 17. Tank with baffles on the inner walls [From Zuo et al. [44], with permission from Elsevier.]

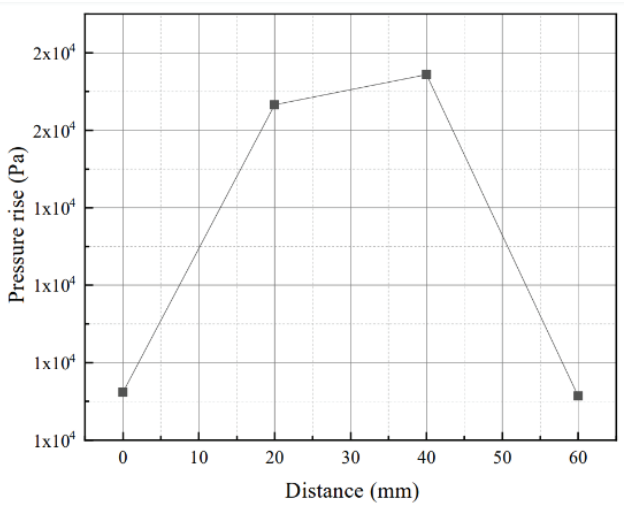

Figure 18. Pressure rise Vs. distance between the adjoining baffles [From Zuo et al. [44], with permission from Elsevier.].

Introduction to cold Helium

This method involves the introduction of cold helium from the bottom up into the tank, through the tor collector. The cold helium in the form of a bubble floats up and blends the heated and cold strata of liquid oxygen (LO_2). This results in an overall reduction in the temperature of the uppermost layer of the propellant or oxidizer [4,75]. This method, even if effective, has a few disadvantages, such as, it aims at reducing the effect caused by heat in-flux and does not deal with the cause of its occurrence. Another disadvantage is that for the storage of the cold helium and for the collector, space and energy are required, which might burden the LV [80–82]. Bubbling of cold Helium (He) is one of the simplest methods to sub-cool the cryogenic fluid in the storage tanks and rocket propulsion applications [28]. To study the effects of bubbling cold helium in cryogenic liquid on the destratification time, a cylindrical tank made from aluminium alloy AA2219, and filled with LN_2, of thickness 5 mm, diameter 400 mm and a height of 915 mm was used for the study [28]. The tank is filled with LN_2 at a temperature of 88 K, up to a height of 755 mm. The tank is pressurized at a constant pressure of 3.0 bar. Prior to bubbling, the tank is kept still for 1000 s, providing enough time for stratification. Bubbling of the gas is done for a duration of 300 s. The effects of different helium mass flow rates (0.1 g s^{-1}, 0.2 g s^{-1} and 0.4 g s^{-1}) on destratification times were analysed. In this study, destratification time is defined as the time taken to drop the fluid temperatures below the stratification limit temperature of 83 K and further to a steady value. It was observed that a total of 6s were required to destratify the LN_2 with GHe flow rate of 0.1 g s^{-1}. By increasing the bubbling gas flow rate by four times, it resulted in a 66.6% reduction in the destratification time. For the range of GHe mass flow rates considered for this study, it was found that the destratification time decreases as GHe mass flow rate increases [28].

CONCLUSION

Thermal stratification, if not controlled, can have severe effects on the functioning of the LVs. Although it is very essential to determine in every case the amount of stratification that can be accepted, its excess reduction can lead to inefficient use of resources, thereby hindering the overall efficiency of the LV.

A few of the important conclusions drawn are as follows:

1. Any degree of thermal stratification, even if it's in the range of 1-2 °C, deteriorates the functioning of the LV.
2. Rotation of the LV tends to slow down the rate of thermal stratification. For a LH_2 tank at 20% fill level, rotating at 1 °/sec in $g/g_0 = 10^{-4}$, under a heat flux of 10 W/m^2 shows a 30 to 60 min reduction in time taken for stratification.
3. An insulation thickness of 40 mm showed the best results, as it had minimum heat in-leak into the storage tank. 40 mm insulation thickness led to a heat in-leak of only 10.7 W/m^2, whereas for the 10mm case a heat in-leak of 64.3 W/m^2 was observed.
4. During the pressurisation phase of the tank, there is a subsequent rise in thermal stratification. Consequently, it has also been reported that with an increase in the ullage pressure from 1 to 4 bar, the liquid-gas interface temperature of liquid Nitrogen rises by up to 9.5%.
5. Novel parameters like λ and T_{sd} have been derived in an attempt to quantify the degree of thermal stratification. T_{sdavg} exhibited a value of 0.20 for a V_g = 0.4 m/s, whereas for 0.8 m/s, T_{sdavg} increased to 0.25, conforming to the observations made, wherein a higher V_g showed better destratification times.
6. Ribs with a pitch-to-height ratio of 1.6 showed promising results among the cases studied. These ribs reduced the degree of stratification by about 30%.
7. Annular baffles along the inner wall of the cryogenic tank also showed promising results. A gap of 60 mm between 2 baffles was deemed optimum and showed a 47% lower pressure rise than that of the 40 mm case.
8. Bubbling of cold Helium gas within the cryogenic tank from its bottom at a rate of 0.1 g s^{-1} took only 6 s of time to bring down the temperature of LN_2 below 83 K. Similarly, simulating bubbling of an inert gas at a velocity of 0.8 m/s from a single orifice, in an 86% filled tank, destratified the tank in 24.95 s.
9. Numerical modelling of an axial jet mixer with a mass flow rate of 3.47 m^3/hr yielded encouraging results as it was successful in mitigating thermal stratification under a time of 8 min within liquid oxygen.

The works reviewed in this article are not only applicable for storage tanks of spacecrafts, but also extend to cryogenic storage tanks used in the thermal industry and thus address a wide array of applications. In the near future, research efforts should be directed and focused more towards reproducing real world conditions in experimental set-ups, which are experienced by the cryogenic storage tanks of LV's during its mission. Replicating such circumstances will substantially improve our understanding of thermal stratification. Furthermore, the combined effects of one or more destratification techniques must also be evaluated in the future.

NOMENCLATURE

D	diameter (m)
DC	drain valve
g	gravitational acceleration (m/s^2)
g/g_0	relative gravity
h	axial distance (m)
H	tank of height (m)
K	kelvin
LRE	liquid rocket engine
LV	launch vehicles
T_U	Ullage temperature (°C)
T_B	Bulk liquid temperature (°C)

T_S	Stratified layer temperature (°C)
CG	Centre of Gravity
LH_2	liquid hydrogen
LO_2	liquid oxygen
LN_2	liquid nitrogen
GHe	Gaseous Helium
P	spacing between ribs (m)
q_w	wall heat flux (W/m^2)
R	tank radius (m)
ΔT	temperature difference
EXS	extruded polystyrene
EPS	expanded polystyrene
d	linear distance between adjoining baffles (m)
VOF	Volume Of Fluid
T	temperature (K)
Q_C	jet flow rate
Q_{BL}	boundary layer flow rate
CFL	Courant Frederick-Levy criteria
T_{sd}	thermal stratification decay coefficient (K/s)
T_{sdavg}	average thermal stratification decay coefficient (K/s)
T_{fin}	ultimate temperature of thermally stratified liquid layer (K)
T_{ini}	original temperature of the thermally stratified liquid layer (K)
t_{ho}	time required for attaining homogeneous temperature distribution (s)
V_g	inlet gas velocity (m/s)

Greek symbols

Ω	angular velocity (°/s)
Ꞥ	spin rate (°/s)
θ_1	upper baffle tilt angle (°)
θ_2	lower baffle tilt angle (°)
δ	distance between baffle and tank wall (m)
λ	thermal stratification parameter

AUTHORSHIP CONTRIBUTIONS

Authors equally contributed to this work.

DATA AVAILABILITY STATEMENT

The authors confirm that the data that supports the findings of this study are available within the article. Raw data that support the finding of this study are available from the corresponding author, upon reasonable request.

CONFLICT OF INTEREST

The author declared no potential conflicts of interest with respect to the research, authorship, and/or publication of this article.

ETHICS

There are no ethical issues with the publication of this manuscript.

STATEMENT ON THE USE OF ARTIFICIAL INTELLIGENCE

Artificial intelligence was not used in the preparation of the article.

REFERENCES

[1] Palerm S, Bonhomme C, Guelou Y, Chopinet JN, Danous P. The future of cryogenic propulsion. Acta Astronaut 2015;112:166–173. [CrossRef]

[2] Fesmire JE, Tomsik TM, Bonner T, Oliveira JM, Conyers HJ, Johnson WL, et al. Integrated heat exchanger design for a cryogenic storage tank. AIP Conf Proc 2014;1573:1365–1372. [CrossRef]

[3] Qiu Y, Yang H, Tong L, Wang L. Research progress of cryogenic materials for storage and transportation of liquid hydrogen. Metals 2021;11:1101. [CrossRef]

[4] Mitikov YO, Ivanenko IS, Pauk OL. New way of eliminating the temperature stratification of liquid oxygen in the tanks of rocket propulsion units. J Aeronaut Aerospace Eng 2017;6:4.

[5] Duan Z, Sun H, Cheng C, Tang W, Xue H. A moving-boundary based dynamic model for predicting the transient free convection and thermal stratification in liquefied gas storage tank. Int J Therm Sci 2021;160:106690. [CrossRef]

[6] Collins Q, Farrington R, Gowie R, Kelly A, Nuzio S, Polus N, et al. Design of thermally efficient cryogenic tanks for spacecraft. In: 2024 Regional Student Conferences 2024;85787. [CrossRef]

[7] Choi SW, Lee WI, Kim HS. Numerical analysis of convective flow and thermal stratification in a cryogenic storage tank. Numer Heat Transf A Appl 2017;71:402–422. [CrossRef]

[8] Feldman Y, Colonius T, Pauken MT, Hall JL, Jones JA. Simulation and cryogenic experiments of natural convection for the Titan Montgolfiere. AIAA J 2012;50:2483–2491. [CrossRef]

[9] Zuo ZQ, Jiang WB, Huang YH. Effect of baffles on pressurization and thermal stratification in cryogenic tanks under micro-gravity. Cryogenics 2018;96:116–124. [CrossRef]

[10] Liu Z, Li Y, Zhou G. Study on thermal stratification in liquid hydrogen tank under different gravity levels. Int J Hydrogen Energy 2018;43:9369–9378. [CrossRef]

[11] Pietrzyk J, Hepworth H. Analysis of thermal stratification in cryogen storage tanks under quiescent, microgravity conditions. In: 27th Joint Propulsion Conference 1991;2327. [CrossRef]

[12] Liu Z, Li Y, Jin Y. Pressurization performance and temperature stratification in cryogenic final stage propellant tank. Appl Therm Eng 2016;106:211–220. [CrossRef]
[13] Xavier M, Raj RE, Narayanan V. Thermal stratification in LH2 tank of cryogenic propulsion stage tested in ISRO facility. IOP Conf Ser Mater Sci Eng 2017;171:012063. [CrossRef]
[14] Agrawal G, Joseph J, Agarwal D, Pisharady JC, Kumar SS. Mathematical modelling of thermal stratification in a cryogenic propellant tank. IOP Conf Ser Mater Sci Eng 2017;171:01204. [CrossRef]
[15] Gupta S, Sharma PK, Kumar S, Tiwari CM. Influence of buoyancy forces in MHD non-Newtonian convective nanofluid utilizing Buongiorno's model induced by 3D exponential sheet. J Therm Eng 2024;10:1107–1119. [CrossRef]
[16] Kumar SP, Prasad BVSSS, Venkatarathnam G, Ramamurthi K, Murthy SS. Influence of surface evaporation on stratification in liquid hydrogen tanks of different aspect ratios. Int J Hydrogen Energy 2007;32:1954–1960. [CrossRef]
[17] Robbins JH, Rogers AC Jr. An analysis on predicting thermal stratification in liquid hydrogen. J Spacecr Rockets 1966;3:40–45. [CrossRef]
[18] Bailey TE, Fearn RF. Analytical and experimental determination of liquid-hydrogen temperature stratification. In: Advances in Cryogenic Engineering 1964;9:254–264. [CrossRef]
[19] Fan SC, Chu JC, Scott LE. Thermal stratification in closed cryogenic containers. In: Advances in Cryogenic Engineering 1969;14:249–257. [CrossRef]
[20] Khurana TK, Prasad BVSSS, Ramamurthi K, Murthy SS. Thermal stratification in ribbed liquid hydrogen storage tanks. Int J Hydrogen Energy 2006;31:2299–2309. [CrossRef]
[21] Yılmaz C, Çetin TH, Öztürkmen B, Kanoglu M. Thermodynamic performance analysis of gas liquefaction cycles for cryogenic applications. J Therm Eng 2019;5:62–75. [CrossRef]
[22] Vishnu SB, Kuzhiveli BT. Effect of roughness elements on the evolution of thermal stratification in a cryogenic propellant tank. In: Kazi SN, editor. Low-Temperature Technologies and Applications. London: IntechOpen; 2021. [CrossRef]
[23] Ryali L, Stautner W, Mariappan D. Impact of internal baffle designs on liquid hydrogen sloshing in cryogenic aircraft fuel tanks. IOP Conf Ser Mater Sci Eng 2024;1301:012068. [CrossRef]
[24] Babaelahi M, Babazadeh MA, Saadatfar M. New design for the cold part of heat pipes using functionally graded material in heat sink with variable thickness fins: An analytical approach. J Therm Eng 2024;10:1323–1334. [CrossRef]
[25] Kumar K, Singh S. Investigating thermal stratification in a vertical hot water storage tank under multiple transient operations. Energy Rep 2021;7:7186–7199. [CrossRef]
[26] Poth LJ, Van Hook JR. Control of the thermodynamic state of space-stored cryogens by jet mixing. J Spacecr Rockets 1972;9:332–336. [CrossRef]
[27] VanOverbeke T. Modeling of pressure reduction due to axial-jet mixers in cryogenic tanks. In: 41st Aerospace Sciences Meeting and Exhibit 2003;998. [CrossRef]
[28] Puthettu Muraleedharan S, Joseph J, Chollackal A, Peter J, Agarwal DK. Experimental investigation of thermal stratification in cryogenic tank subjected to multi-species bubbling. J Therm Anal Calorim 2023;148:2949–2959. [CrossRef]
[29] Oliveira J, Kirk DR, Schallhorn PA, Piquero JL, Campbell M, Chase S. An improved model of cryogenic propellant stratification in a rotating, reduced gravity environment. In: NASA Thermal and Fluids Analysis Workshop (TFAWS) Conference 2007;1–20.
[30] Liu Z, Wang L, Jin Y, Li Y. Development of thermal stratification in a rotating cryogenic liquid hydrogen tank. Int J Hydrogen Energy 2015;40:15067–15077. [CrossRef]
[31] Oliveira J, Kirk DR, Schallhorn PA. Analytical model for cryogenic stratification in a rotating and reduced-gravity environment. J Spacecr Rockets 2009;46:459–465. [CrossRef]
[32] Saunders KD, Beardsley RC. An experimental study of the spin-up of a thermally stratified rotating fluid. Geophys Astrophys Fluid Dyn 1975;7:1–27. [CrossRef]
[33] Liu Z, Wang L, Jin Y, Li Y. Development of thermal stratification in a rotating cryogenic liquid hydrogen tank. Int J Hydrogen Energy 2015;40:15067–15077. [CrossRef]
[34] Zhang M, Liu Q, Tao Y, He N, et al. Research on interfacial flow and thermal stratification of cryogenic liquid nitrogen in variable gravity. Chin J Space Sci 2024;44:846–862. [CrossRef]
[35] Onosovskii EV, Stolper LM, Kulik NA, Kostritskii VY. Selection of the optimum type and thickness of insulation for cryogenic tanks. Chem Pet Eng 1984;20:309–313. [CrossRef]
[36] Agrawal G, Joseph J, Agarwal DK, Kumar SS. Effect of insulation thickness on evolution of pressure and temperature in a cryogenic tank. In: Proc 23rd Natl Heat Mass Transfer Conf and 1st Int ISHMT-ASTFE Heat Mass Transfer Conf. 2015:17–20.
[37] Mzad H, Haouam A. Optimization approach of insulation thickness of non-vacuum cryogenic storage tank. Prog Supercond Cryog 2020;22:17–23.
[38] Joseph J, Agrawal G, Agarwal DK, Pisharady JC, Kumar SS. Effect of insulation thickness on pressure evolution and thermal stratification in a cryogenic tank. Appl Therm Eng 2017;111:1629–1639. [CrossRef]
[39] Kürekci NA. Optimum insulation thickness for cold storage walls: Case study for Turkey. J Therm Eng 2020;6:873–887. [CrossRef]

[40] Shahid M, Karimi MN, Mishra AK. Optimum insulation thickness for external building walls for different climate zone in India. J Therm Eng 2024;10:1198−1211. [CrossRef]
[41] Kang M, Kim J, You H, Chang D. Experimental investigation of thermal stratification in cryogenic tanks. Exp Therm Fluid Sci 2018;96:371−382. [CrossRef]
[42] Scheufler H, Gerstmann J. Heat and mass transfer in a cryogenic tank in case of active-pressurization. Cryogenics 2022;121:103391. [CrossRef]
[43] Schmidt AF, Purcell JR, Wilson WA, Smith RV. An experimental study concerning the pressurization and stratification of liquid hydrogen. In: Advances in Cryogenic Engineering 1960;5:487−497. [CrossRef]
[44] Zuo ZQ, Jiang WB, Huang YH. Effect of baffles on pressurization and thermal stratification in cryogenic tanks under micro-gravity. Cryogenics 2018;96:116−124. [CrossRef]
[45] Chin JH, Harper EY, Hines FL, Hurd SE, Vliet GC. Analytical and experimental study of stratification and liquid-ullage coupling. NASA Report No. LMSC-2-05-65-1. 1965.
[46] Sunena S. Better propulsion system for next generation space travel. J Aeronaut Aerospace Eng 2021;10:262.
[47] Moran ME. Cryogenic fluid storage technology development: Recent and planned efforts at NASA. NASA Report No. E-16816. 2009.
[48] Hermsen R, Zandbergen B. Pressurization system for a cryogenic propellant tank in a pressure-fed high-altitude rocket. In: 7th European Conference for Aeronautics and Aerospace Sciences 2017;1−13.
[49] Kassemi M, Kartuzova O. Effect of interfacial turbulence and accommodation coefficient on CFD predictions of pressurization and pressure control in cryogenic storage tank. Cryogenics 2016;74:138−153. [CrossRef]
[50] Means JD, Ulrich RD. Transient convective heat transfer during and after gas injection into containers. J Heat Transf 1975;97:282−287. [CrossRef]
[51] Raval P, Ramani B. Heat transfer enhancement techniques using different inserts in absorber tube of parabolic trough solar collector: A review. J Therm Eng 2024;10:1068−1091. [CrossRef]
[52] SB V, Bhowmick S, Kuzhiveli BT. Experimental and numerical investigation of stratification and self pressurization in a high pressure liquid nitrogen storage tank. Energy Sources Part A 2022;44:2580−2594. [CrossRef]
[53] Wang J, Webley PA, Hughes TJ. Thermodynamic modelling of low fill levels in cryogenic storage tanks for application to liquid hydrogen maritime transport. Appl Therm Eng 2024;256:124054. [CrossRef]
[54] Fard MA, Barkdoll B. Simple device to improve mixing in storage tanks. In: World Environmental and Water Resources Congress 2019;2019:528−535. [CrossRef]
[55] Dash S, Singh N. Effects of partial heating of top rotating lid with axial temperature gradient on vortex breakdown in case of axisymmetric stratified lid driven swirling flow. J Therm Eng 2016;2:883−896. [CrossRef]
[56] Shad M, Kamran MA. Investigation of the thermal performance of cryogenic regenerator as a porous structure. J Therm Eng 2016;2:962−970. [CrossRef]
[57] Paul A, Nath JM, Das TK. An investigation of the MHD Cu-Al_2O_3/H_2O hybrid-nanofluid in a porous medium across a vertically stretching cylinder incorporating thermal stratification impact. J Therm Eng 2023;9:799. [CrossRef]
[58] Bayareh M. Study of the effect of the porous plates on the tank bottom on the boiling process. J Therm Eng 2019;5:149−156. [CrossRef]
[59] Perona JJ, Hylton TD, Youngblood EL, Cummins RL. Jet mixing of liquids in long horizontal cylindrical tanks. Ind Eng Chem Res 1998;37:1478−1482. [CrossRef]
[60] Brodnick JM, Williams BR, Reske EJ. Validation of a computational fluid dynamics model of axial jet mixing for cryogenic propellant tank pressure control. In: AIAA SciTech Forum and Exposition 2024;1−12.
[61] Raj S, Bibin KS, Roy KER, Prasad B, Jayakumar JS. Analysis of thermal stratification decay in liquid storage tanks using OpenFOAM. 2024;1−81. [CrossRef]
[62] Lan E, Shi S. Coupled modeling and simulation of tank self-pressurization and thermal stratification. Int J Heat Mass Transf 2024;232:125885. [CrossRef]
[63] Fu J, Sunden B, Chen X. Influence of wall ribs on the thermal stratification and self-pressurization in a cryogenic liquid tank. Appl Therm Eng 2014;73:1421−1431. [CrossRef]
[64] Akinshilo A. Analytical decomposition solutions for heat transfer on straight fins with temperature dependent thermal conductivity and internal heat generation. J Therm Eng 2019;5:76−92. [CrossRef]
[65] Elmouazen H, Zhang X, Gibreel M, Ali M. Heat transfer enhancement of hydrogen rocket engine chamber wall by using V-shape rib. Int J Hydrogen Energy 2022;47:9775−9790. [CrossRef]
[66] Attou Y, Bouhafs M, Feddal A. Numerical analysis of turbulent flow and heat transfer enhancement using V-shaped grooves mounted on the rotary kiln's outer walls. J Therm Eng 2023;10:350−359. [CrossRef]
[67] Li X, Zhang S, Qin J, Bao W. Regulation mechanism of microribs on heat transfer process of cracking reactive flow with strong thermal stratification. J Heat Transf 2020;142:114501. [CrossRef]
[68] Madani K. Numerical investigation of cooling a ribbed microchannel using nanofluid. J Therm Eng 2018;4:2408−2422. [CrossRef]

[69] Gibreel M, Zhang X, Elmouazen H. Investigation of heat transfer enhancement and thermal stratification phenomenon on supercritical hydrogen fuel flow. Therm Sci Eng Prog 2024;53:102759. [CrossRef]
[70] Yıldırım C. Theoretical investigation of a solar air heater roughened by ribs and grooves. J Therm Eng 2018;4:1702−1712. [CrossRef]
[71] Noor D, Mırmanto H, Sarsetiyanto J, Soedjono D. Flow behavior and thermal separation mechanism on vortex tube. J Therm Eng 2021;7:1090−1099. [CrossRef]
[72] Ahmadi Nadooshan A, Jahanbakhshi A, Bayareh M. Geometry effects on thermohydraulic behavior of fluid flow in a square enclosure with an inner circular tube. J Therm Eng 2019;5:138−148. [CrossRef]
[73] Grayson G, Lopez A, Chandler F, Hastings L, Tucker S. Cryogenic tank modeling for the Saturn AS-203 experiment. In: 42nd AIAA/ASME/SAE/ASEE Joint Propulsion Conference & Exhibit 2006;5258. [CrossRef]
[74] Tunc G, Wagner H, Bayazitoglu Y. Space shuttle upgrade liquid oxygen tank thermal stratification. In: 35th AIAA Thermophysics Conference 2001;3082. [CrossRef]
[75] Liu Z, Yang Y, Liu Y, Li Y. Effect of gas injection mass flow rates on the thermal behavior in a cryogenic fuel storage tank. Int J Hydrogen Energy 2022;47:14703−14713. [CrossRef]
[76] Dec JE, Hwang W. Characterizing the development of thermal stratification in an HCCI engine using planar-imaging thermometry. SAE Int J Engines 2009;2:421−438. [CrossRef]
[77] Daigle MJ, Smelyanskiy VN, Boschee J, Foygel M. Temperature stratification in a cryogenic fuel tank. J Thermophys Heat Transf 2013;27:116−126. [CrossRef]
[78] Walls LK, Kirk D, deLuis K, Haberbusch MS. Experimental and numerical investigation of reduced gravity fluid slosh dynamics for the characterization of cryogenic launch and space vehicle propellants. In: Cryogenic Engineering Conference 2011;136. [CrossRef]
[79] Fakiri F, Rahmoun K. Unsteady numerical simulation of turbulent forced convection in a rectangular pipe provided with waved porous baffles. J Therm Eng 2017;3:1466−1477. [CrossRef]
[80] Schallhorn P, Campbell D, Chase S, Piquero J, Fortenberry C, Li X, et al. Upper stage tank thermodynamic modeling using SINDA/FLUINT. In: 42nd AIAA/ASME/SAE/ASEE Joint Propulsion Conference & Exhibit 2008;5051.
[81] Bolshinskiy LG, Hedayat A, Hastings LJ, Moder JP, Schnell AR, Sutherlin SG. TankSIM: A cryogenic tank performance prediction program. In: Space Cryogenics Workshop 2015;M15-4803.
[82] Jurns JM, Tomsik TM, Greene WD. Testing of densified liquid hydrogen stratification in a scale model propellant tank. In: 1999 Cryogenic Engineering and International Cryogenic Materials Conference 2001;TM-2001-209391.
[83] Cimbala JM. Fluids in rigid body motion. Available at: https://www.me.psu.edu/cimbala/Learning/Fluid/Rigid_body/rigid_body.htm. Accessed July 16, 2025.